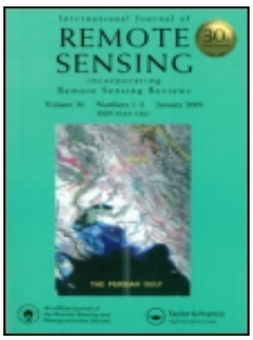

International Journal of Remote Sensing

ISSN: 0143-1161 (Print) 1366-5901 (Online) Journal homepage: https://www.tandfonline.com/loi/tres20

A water index for rapid mapping of shoreline changes of five East African Rift Valley lakes: an empirical analysis using Landsat TM and ETM+ data

Yashon O. Ouma & R. Tateishi

To cite this article: Yashon O. Ouma & R. Tateishi (2006) A water index for rapid mapping of shoreline changes of five East African Rift Valley lakes: an empirical analysis using Landsat TM and ETM+ data, International Journal of Remote Sensing, 27:15, 3153-3181, DOI: 10.1080/01431160500309934

To link to this article: https://doi.org/10.1080/01431160500309934

International Journal of Remote Sensing
Vol. 27, No. 15, 10 August 2006, 3153–3181

Taylor & Francis
Taylor & Francis Group

A water index for rapid mapping of shoreline changes of five East African Rift Valley lakes: an empirical analysis using Landsat TM and ETM+ data

YASHON O. OUMA*† and R. TATEISHI‡

†Graduate School of Science and Technology, Chiba University, 1-33 Yayoi, Inage-ku, Chiba, 263-8522, Japan

‡Centre for Environmental Remote Sensing, Chiba University, 1-33 Yayoi, Inage-ku, Chiba, 263-8522, Japan

(*Received 23 January 2005; in final form 11 August 2005*)

Because of the complicated shorelines, inaccessibility and vast spread of some lakes, information on changing shorelines is difficult to acquire. A new water index (WI) has been applied to quantify changes in five saline and non-saline Rift Valley lakes in Kenya using Landsat Thematic Mapper (TM) and Enhanced Thematic Mapper (ETM+) data. The WI is based on a logical combination of the Tasseled Cap Wetness (TCW) index and the Normalized Difference Water Index (NDWI). Using regression analysis with estimated shoreline coordinates, the WI detected the shorelines with an accuracy of 98.4%, which was 22.3% higher than the TCW, and 43.2% more accurate than the NDWI. Change detection was derived using image differencing followed by density slicing and unsupervised classification. The saline lakes (Bogoria, Nakuru and Elementaita) changed more with respect to the ratio of the change in the original surface areas than the non-saline lakes (Baringo and Naivasha).

1. Introduction

The delineation and extraction of coastline or shoreline of rivers and lakes is an important task that has application in different fields such as lake/coastline erosion monitoring, lake/coastal-zone management, watershed definition, flood prediction and evaluation of water resources. This task is difficult, time-consuming, and sometimes impossible for a huge region such as an entire country or continent, when using traditional ground survey techniques. This is because water bodies can be very large, have very complex shorelines, may be fast moving as in floods, tides and storm surges, or may be inaccessible. In addition, automatic and replicable techniques are required to update coastline/shoreline maps, evaluate the spatial and temporal evolutions and sensitivities of alterations due to natural and anthropic events (Bagli and Soille 2003).

Following the increase in the availability of satellite images, the development of tools for geographic data analysis (Geographic Information Systems (GIS) platforms) and image processing techniques, numerous research studies have attempted to extract and delineate water bodies from these images (Smith 1997). The extraction of features such as coastlines and water bodies directly from satellite

*Corresponding author. Email: yashon@graduate.chiba-u.jp

International Journal of Remote Sensing
ISSN 0143-1161 print/ISSN 1366-5901 online
http://www.tandf.co.uk/journals
DOI: 10.1080/01431160500309934

images overcomes the problem of matching available coastline/shoreline datasets with the image dataset studied. However, because of projection system biases, the matching of a shoreline coming from a different dataset with the available images may turn out to be a very time-consuming, if not impossible, task. Beyond manual digitization, several techniques have been reported in the literature for the derivation of the coastline position from satellite images (Bagli and Soille 2003). The most common are density slice using single or multiple bands and multispectral classification, both supervised and unsupervised (e.g. ISODATA-unsupervised classification, principal components analysis (PCA), Tasseled Cap Wetness (TCW), Normalized Difference Water Index (NDWI), maximum-likelihood supervised classification).

In recent years, satellite remote sensing data have been used in automatic or semi-automatic shoreline extraction and mapping (Di *et al.* 2003). Braud and Feng (1998) evaluated threshold level slicing and multispectral image classification techniques for detection and delineation of the Louisiana shoreline from 30-m resolution Landsat Thematic Mapper (TM) imagery. They found that thresholding TM band 5 was the most reliable methodology. Jupp *et al.* (1985) analysed the histogram of Landsat TM band 7 and segmented water pixels by thresholding. Moller-Jensen (1990) performed the thresholding in TM bands 4 and 5 and then recognized water pixels using experience-based rules. McFeeters (1996) detected water bodies using the NDWI. Synthetic aperture radar (SAR) imagery has also been used to extract shorelines for various geographic locations (Niedermeier *et al.* 2000, Schwäbisch *et al.* 2001).

Frazier and Page (2000) have reviewed several approaches used by different authors to delineate water bodies from Landsat TM and Multispectral Scanner (MSS) classification. They found that simple density slicing of the TM band 5 (mid-infrared) successfully detected lake/pond wetland areas, achieving a classification accuracy of 96.9%, in the Wagga Wagga region of Australia, but failed to extract small water bodies adequately. Simple density slicing of Landsat TM bands 4 and 7 give a good water classification result but with low accuracy with respect to band 5. Zhu (2001) used a neural network classifier on multitemporal Landsat images to classify the changes of coastline in different periods. Di *et al.* (2003) investigated a novel approach for automatic extraction of shorelines from high-resolution IKONOS satellite imagery using a mean shift segmentation algorithm as a first step, and then a local refinement process.

Most of these approaches are highly reliant on (a) human expertise and local area knowledge and (b) accurate radiometric and geometric correction for shoreline mapping and water bodies change derivation. Detection of water bodies *per se* is not the difficult task. The problem is the accurate or exact delineation of the water body shoreline (the 'true' land–water interface) at a certain time. 'True' here means the lake edge not influenced by wind flows, water currents, dune juxtapositions or shadows, among other factors that may influence the true edge information extraction and change detection procedure. Furthermore, there has been no robust documentation on the broadband Landsat reflectance especially for lake shoreline mapping and change detection. Most of the work so far has concentrated on water quality, for example turbidity aspects (Fraser 1998).

In general, supervised classification techniques, based on spectral signature analysis, lead to good results in delineating and extracting large water boundaries from remote sensed data, but these methods meet some problems if the aim is to perform a rapid and reproducible (reliable) extraction of shorelines that is valid for a

huge area such as a mosaic of Landsat images covering a locality, country or even a continent.

In the case of disasters such as flooding, the delivery of geospatial data and information is expected in much shorter time periods. In such scenarios three main rapid mapping requirements are expected to be dealt with: (a) recognition of features, (b) extraction of features, and (c) change detection, including correction to existing features. All require extensive human involvement, and they are time-consuming operations. Considering the continuous dwindling resources (human, budgets) and the vast size of shorelines, there is a need to implement rapid mapping approaches to reduce both the production time and the cost involved. These approaches require not only revisiting the current processes or techniques used but also, and most importantly, the implementation of a higher level of automation in the mapping operations.

In principle, the use of spectral sensors should solve the problem of representativity in *in situ* point-to-point measurements. Statistical spatial measures describing landscape characteristics and water bodies have not been widely adapted to remote sensing data and to collecting data and information on the state of the water environment.

In this paper, we propose a new, simple, fast and accurate methodology based on a combination of the two indices TCW and NDWI for shoreline delineation and change mapping. The methodology is applied to five lakes within one Landsat scene (path 169, row 060) covering part of the Kenyan portion of the East African Rift Valley. This combined formulation is called the water index (WI). Based on Landsat TM and Landsat Enhanced Thematic Mapper (ETM+) imagery, dated 1986 and 2001, respectively, the new approach was investigated and calibrated using Lake Nakuru as the test lake, and the concept extended to the scene containing five lakes. By combining the two indices, the problems of fuzzy shoreline and errors in lake extent (surface area) and change detection are minimized. Simple differencing and density slicing were used to derive the change information. The methodology has the advantage of avoiding extensive thresholding as reported in previous studies. The results are very promising following extensive empirical, ground measurements and statistical comparisons.

2. Study area and data

The study area outlined in figure 1 contains five of the lakes within the East African Rift Valley, namely Lakes Baringo, Bogoria, Nakuru, Elementaita and Naivasha. This are extends from N 00°36′, E 36°01′ to S 00°47′, E 36°23′. Three of the lakes (Bogoria, Nakuru and Elementaita) are saline; the other two are non-saline. The data used in this study were taken from 28 January 1986 for Landsat TM and 3 April 2001 for Landsat ETM+. This is a Landsat scene (path 169, row 060) and contains the five lakes investigated in this study.

3. Methodology

3.1 *Geometric and radiometric data correction*

Geometric correction is a methodology for rectifying the common areas test data to the same or required projection system, for producing spatially correct land cover information. The study data were geometrically rectified to the Universal Transverse Mercator (UTM) map projection system, zone 37 East, using 120 ground control points (GCPs) evenly distributed within the 2001 Landsat ETM+ scene. A 1997

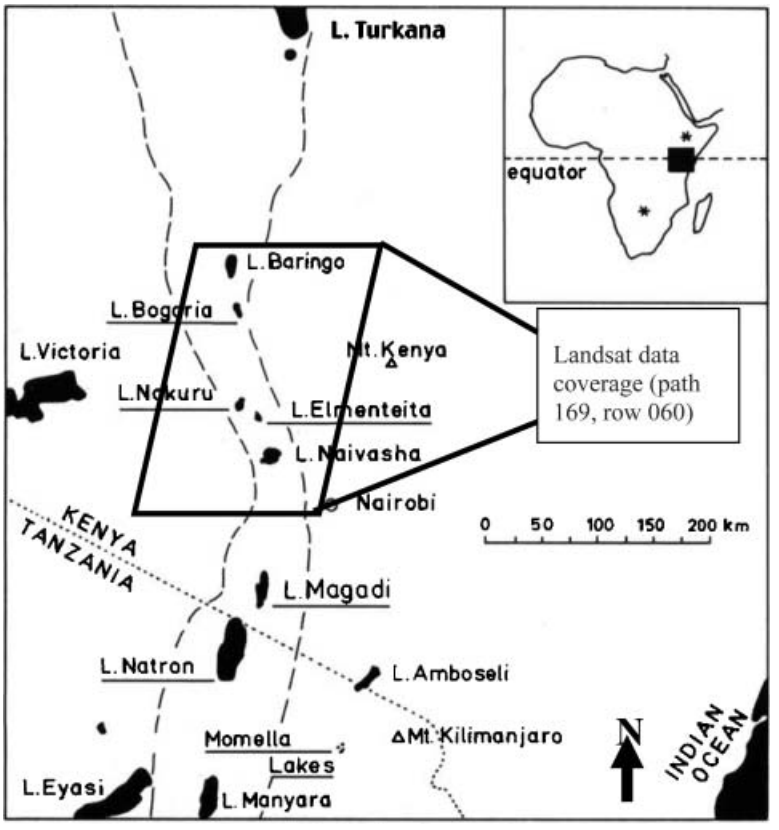

Figure 1. Location map of study area within landsat data coverage (path 169, row 060).

topographic map of the study area, at a scale of 1 : 50 000, was used to geometrically rectify the Landsat 7 (ETM+) data to an accuracy of about half a pixel (15 m).

The geometrically corrected ETM+ data were used to rectify the Landsat 5 (TM) image by the image-to-image registration method. A first-degree polynomial equation was used in the image transformation. A nearest-neighbour resampling method was used to resample the TM to the same spatial resolution as ETM+ ($30\,m \times 30\,m$) to allow for pixel-to-pixel comparison and to avoid altering the original pixel values of the images. To normalize these datasets for change detection (i.e. remove unnecessary artefacts or noise), pseudo-invariant (i.e. temporally unchanged) features on the ground and image were used to normalize across the images concurrently. A Differential Global Positioning System (DGPS) was used to collect positional (XY) data in 2000/2001 for the assessment of the shoreline and true location of the checkpoints, for validation of the ETM+-derived shoreline. This time frame was chosen because the shoreline does vary sometimes based on seasonal-climatic changes.

Based on local knowledge of the lake, apart from seasonal-climatic induced changes, the level and hence the surface area change regularly on the relatively flatter western side because of daily wind speed variations as well as lake currents. Consistent and redundant DGPS observations are therefore essential for obtaining proximate lake edge information, especially before proceeding with the change detection exercise. The shallow edges of the lake represent the dynamic edge region,

which may be unreliable for true long-term change detection. For this study, DGPS measurements were taken before the season changed from the dry (December 2000 to February 2001) to the wet season (March 2001 onwards). This was to establish the proximate true edge for comparison with the satellite overpass information and for the subsequent change detection. Only the overlapping points (i.e. with the same coordinates) with accuracies within the 30 m spatial resolution of the Landsat test data were used in the validation process. Similar limitations with regard to reliable GPS measurements were reported by Fraser (1998).

3.2 *Tasseled Cap Wetness (TCW)*

The concept of tasseled cap transformation is a useful tool for compressing spectral data into a few bands associated with physical scene characteristics (Crist and Cicone 1984). It was originally constructed for understanding the phenomena of crop development in spectral space (Kauth and Thomas 1976). The tasseled cap transformation in remote sensing is the conversion of the readings in a set of channels into composite values through weighted sums of separate channel readings.

The tasseled cap transformation of Landsat TM and ETM+ consists of six multispectral features, all of which could be potentially differentiated in terms of stability and change in a multitemporal data set. Three of the six tasseled cap transform bands are often used: band 1 (brightness, measure of soil), band 2 (greenness, measure of vegetation) and band 3 (wetness, interrelationship of soil and canopy moisture). These first three features usually account for the most variation in a single-date image (Crist 1985, Crist and Kauth 1986, Cohen *et al.* 2001, Collins and Woodcock 2001). The TCW for Landsat satellite imagery is calculated with the following coefficients (equation (1)):

$$\mathrm{TCW}=0.1509(\rho_1)+0.1973(\rho_2)+0.3279(\rho_3)+0.3406(\rho_4)-0.7112(\rho_5)-0.4572(\rho_7) \quad (1)$$

where (ρ_i) corresponds to the respective Landsat TM and ETM+ bands.

3.3 *Normalized difference water index (NDWI)*

The concept of the NDWI in the delineation of open water features was first introduced by McFeeters (1996). In this study we propose to estimate the NDWI by evaluating different NDWIs based on the different spectral bands of TM and ETM+ (equations (2)–(6)). NDWI_1 is based on the mid-infrared (MIR) and shortwave infrared (SWIR) bands 5 and 7. NDWI_2 is based on the near-infrared (NIR) band 4 and visible (green) band 2. NDWI_3 is computed from the NIR band 4 and MIR band 5. NDWI_4 is calculated based on the MIR band 5 and visible (green) band 2. NDWI_5 is based on the SWIR band 7 and visible (green) band 2.

$$\mathrm{NDWI}_1=\frac{\rho_7-\rho_5}{\rho_7+\rho_5} \quad (2)$$

$$\mathrm{NDWI}_2=\frac{\rho_4-\rho_2}{\rho_4+\rho_2} \quad (3)$$

$$\mathrm{NDWI}_3=\frac{\rho_5-\rho_4}{\rho_5+\rho_4} \quad (4)$$

$$\mathrm{NDWI}_4 = \frac{\rho_5 - \rho_2}{\rho_5 + \rho_2} \tag{5}$$

$$\mathrm{NDWI}_5 = \frac{\rho_7 - \rho_2}{\rho_7 + \rho_2} \tag{6}$$

The existing NDWI (e.g. McFeeters 1996) is based on evaluation of the spectral signature in the near- and mid-infrared portions of the electromagnetic spectrum. In this range the water bodies absorb almost all incident radiant flux while the land surface reflects significant amounts of near- and mid-infrared energy. However, the shallow water–land interface presents mixed reflectance depending on the type of suspended solid particles in the shallow end of the lake, how deep they are around the lake edge and the mobility of the water mass. This index has been used mainly within the scope of water quality parameters assessment (Fraser 1998) and not in fluctuations in lake size over long time intervals. The reliability of this NDWI for lake size mapping and change detection is thus not robustly established in the literature. This suggests that further consideration of the visible and shortwave infrared wavelengths may be necessary to determine the true lake edge. The rationale for testing these different spectral domains is that preliminary assessments showed that all the indices, equations (2)–(6), have the potential to detect the presence of open water bodies. However, for exact delineation of the shoreline, it is not clear which of the indices is most accurate or reliable, or whether multiple NDWI indices might be more suitable. In general, mapping of open water bodies such as lakes is not difficult. The challenge is in the optimal determination of the actual shoreline (true land–water interface), which is fuzzy in most cases. Thresholding, although widely used, may not be suitable where rapid edge detection is required.

3.4 *Methodology for test case using Lake Nakuru*

We first illustrate the performance of each of the NDWI and TCW by comparing results from ETM+ data for Lake Nakuru, for different portions of the lake with interesting features/characteristics. Lake Nakuru was chosen for the test because it is the most fluctuating lake in size, with a more complex shoreline structure. In addition, the authors have a good physical knowledge of the lake. Extensive fieldwork was used in this part of the study to verify what was observed on the image or to select the desired portions of the lake.

The results of the TCW and the five NDWIs are presented in figures 2(*a*) and 2(*b*)–2(*f*), respectively. TCW results (figure 2(*a*)) delineate the lake outline very well, but include the sewage plants. The sewage plants are reflecting like the water body on the northwestern side of the lake. Comparing the entire scene, the water body is well delineated with bright pixels. A visual comparison of NDWI results shows that NDWI_3 and NDWI_4 present a nearly similar output. The difference is that a buffer is formed around the lake in the case of NDWI_4 and a precise demarcation of the shoreline is demonstrated by NDWI_3. With NDWI_1, not only is the shoreline imprecisely outlined but also the lake pixels as a whole are not properly aggregated. A similar buffer as in NDWI_4 is observed in NDWI_2 and NDWI_5. The problem in the latter two results is that they retain a lot of noise in the form of non-water information, which may make any further analysis of the scenes difficult as compared to NDWI_3 and NDWI_4. Although NDWI_3 retained some noise within the

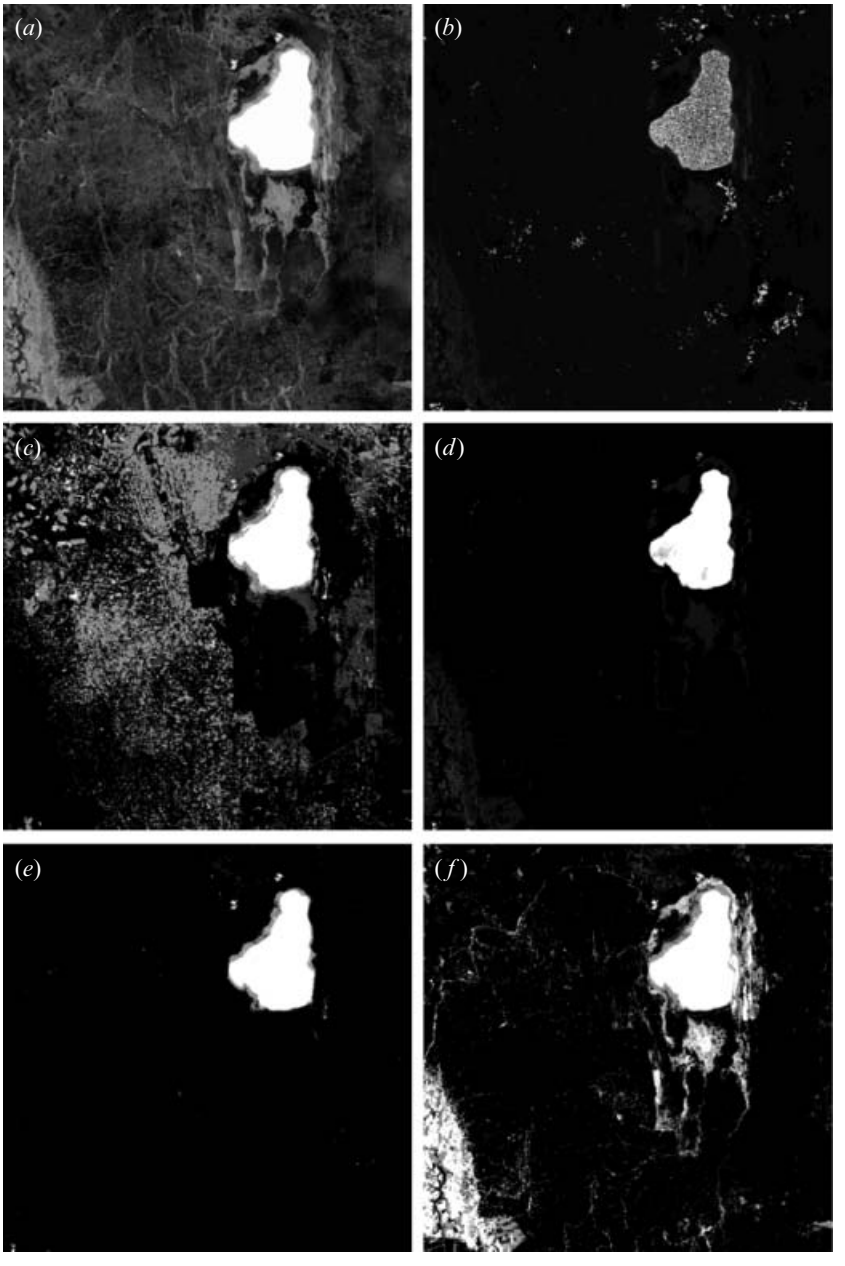

Figure 2. Results of (*a*) TCW and (*b–f*) $NDWI_{1–5}$ for Lake Nakuru.

lake, it presented much clearer or non-fuzzy edge information representing the true edge of the lake boundary compared to the rest of the NDWIs. As is demonstrated in the following sections, a combinational approach of the optimal or most informative NDWI and TCW, based on a set of rules, eliminates the noise within the $NDWI_3$. This is one of the advantages of the approach presented in this study.

The mixed pixels within the scene representing non-water are indicators of the degree of the wetness of the scene features as detected by the respective indices. The brightest pixels depict 100% wetness, that is water only, while the darkest pixels

depict 0% wetness, meaning no water or a very low water content. This method is important in its ability to suppress the non-water pixels completely or as much as possible, while accurately enhancing the lake water body and the shoreline.

Natural lake currents, wind motions/directions and dune juxtaposition influence the shallow edges, also referred to here as 'unreliable edges'. The shallow edges thus keep fluctuating irregularly (Fraser 1998). Depending on the index, the shallow edges form a dynamic or non-stationary buffer zone around the true edges. For example, from the results presented in figure 2, it is apparent that all the indices except $NDWI_3$ present a buffer zone around the shallow edge of the lake. The problem is that for a wider scene, the values of some of these buffer zone digital numbers (DNs) are similar to those of other shallow water marshes within the scene, which could be smaller than the lake. Thus the problem of accurate edge arises. In this study, only the extraction of the 'true-edge' was considered and the DGPS measurements were based on this true 'true-edge', or fairly stationary edge.

3.5 *Comparison of test case TCW and NDWI results*

To evaluate the significance of the results, we empirically analysed the results of the NDWIs independently and then compare them with TCW. We selected unique sections of the lakeshore: (i) point of river entry into lake (A); (ii) most irregular, complicated shoreline portions of the lake (B); (iii) long narrow strip of the lake–mountain (cliff) edge (C); and (iv) where there is widespread water plants and algal bloom (like A and C) in the lake. In figure 3(*a*) (false colour composite of ETM+ bands 4, 5 and 7), sections A, B and C of the lake are marked out. The rationale for comparing the indices is to determine the optimal indices that are informative enough to depict the 'true-edge' information. This provides for redundancy where there is overlap in information content, resulting in enhancement and more accurate detection and isolation of the feature of interest.

3.5.1 River–lake confluence (portion A). In figure 3(*b*), the significant point of assessment is the point of entry of a river into the lake and the subsequent sediment deposits, algal bloom and general lake surface instability around this part. This phenomenon is also observable in other similar portions of the lake. This implies that the reflectance here will be different from that of the lake, even though it is lake-water. The objective is to identify which of the NDWIs best estimates such a portion of the lake (circled region as in figure 3(*b*), zoom section of portion A) by accurately defining the shoreline and including the red tone area as part of the lake.

The results for $NDWI_1$ were not assessed further because, as observed from the results in figure 2(*b*), it is not possible to extract the lake accurately, leaving the shoreline alone. The rest of the NDWI results for portion A are shown in figures 3(*c*)–3(*f*).

All the NDWI results present different shorelines. This is the problem when a user decides to use a specific NDWI before comparing with other alternatives. Comparing these results to the original image, figure 3(*b*), and field data, while focusing on the portion of interest, we found that: (a) $NDWI_2$ overestimated the true shoreline; (b) $NDWI_3$ estimated the shoreline in such a way that we had to decide whether to include the pixels defining the confusing portion (A). In other words, $NDWI_3$ gave good results around this section, separating pure water and impure water. However, these pixels are similar to others within the scene. Thus a manual approach would have to be adapted to threshold out non-water pixels. This

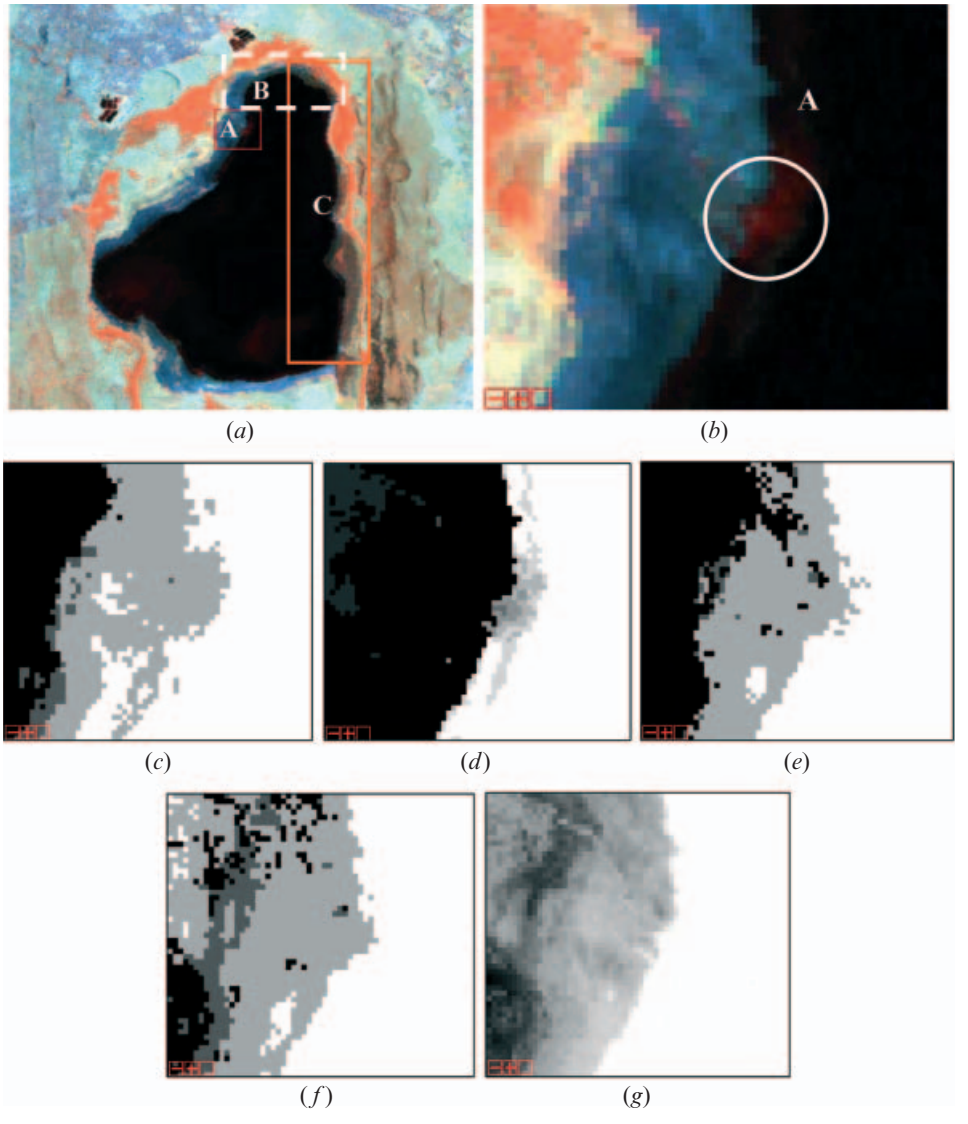

Figure 3. (*a*) Location of test areas A–C in FCC and (*c–f*) results of $NDWI_{2–5}$ and (*g*) TCW of (*b*) test area A of Lake Nakuru.

was not our desired objective, as we envisaged a more automated, rapid approach with minimal error. (c) $NDWI_4$ and $NDWI_5$ underestimated the shoreline not only by excluding the test portion but also by including non-water pixels (as bright pixels with the same DNs) within the scene. Hence, for this portion of the study, we concluded that $NDWI_3$ gave the best result, as it accurately estimated the shoreline and also took care of the presence of disturbances in this part of the lake, so that further processing may yield better results.

The TCW results for this section are presented in figure 3(*g*). Comparing the region of interest between the two indices (TCW and NDWI), it is clear that the TCW recognized this confusing portion as part of the pure water. Only the results from $NDWI_3$ are comparable to those of TCW. The apparent difference is that

NDWI gives a crisp definition of the shoreline as compared to the near-fuzzy shoreline delineated by TCW. Thus, an improvement on the results of TCW also requires further post-processing such as thresholding with density slicing. Inspecting the two images, we found that they exhibited a similar flow pattern of the shoreline. This is a good indicator of the reliability of shoreline definition from the two methods.

3.5.2 Irregular and complicated shoreline (portion B). Portion B, representing a complicated and very irregular shoreline, was analysed in order to depict the suitability of the two approaches. In this section, a narrow extension of the lake into land makes it difficult to map the shoreline due to mixed pixels caused by obscuring

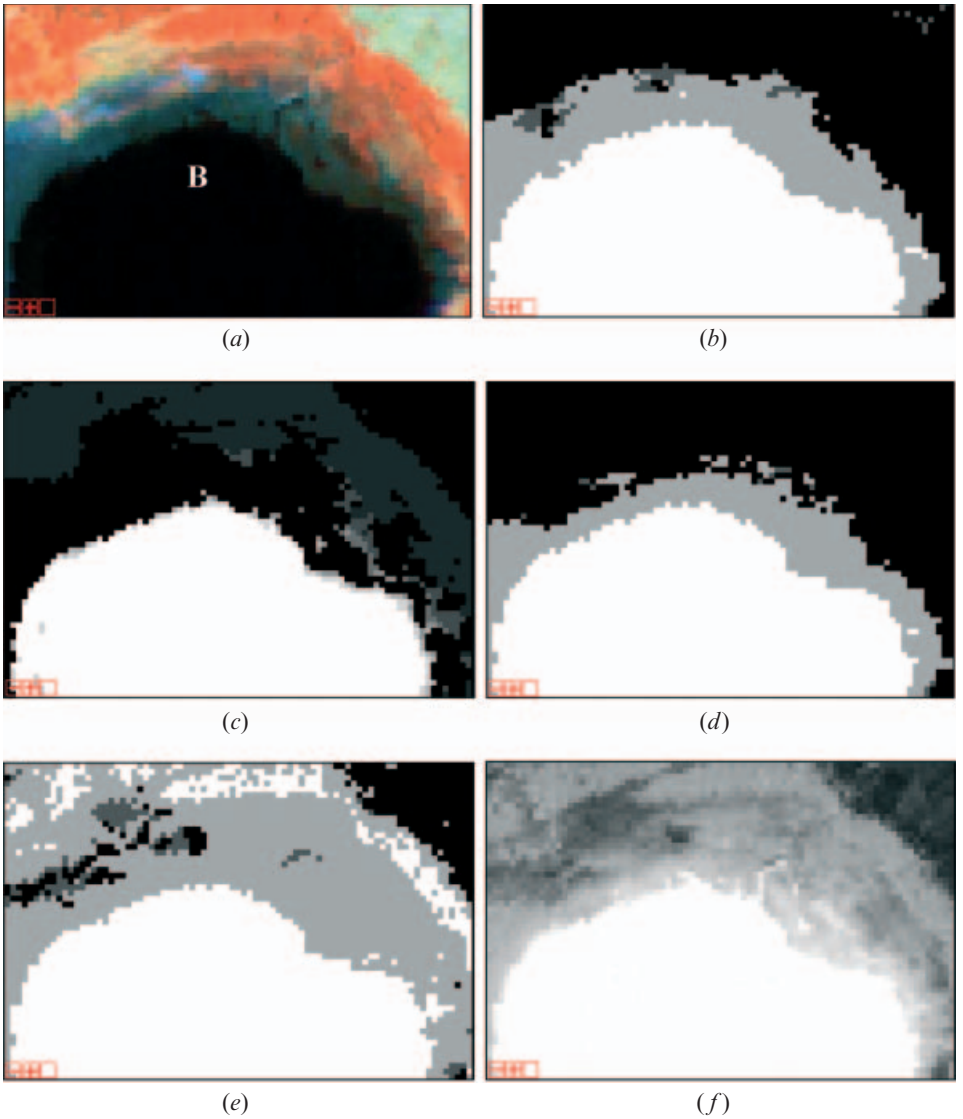

Figure 4. (*a*) Location of test area B in FCC; (*b–e*) results of $NDWI_{2-5}$ and (*f*) TCW of Lake Nakuru.

of the very narrow shoreline by overhanging land, shadows and trees. Figure 4(*a*) shows the original image-portion of section B. The NDWI results for $NDWI_{2–5}$ are presented respectively in figures 4(*b*)–4(*e*). The results of $NDWI_1$ are omitted as they are the poorest.

Figure 4(*b*) shows that $NDWI_2$ underestimated the shoreline by defining a perfect shoreline but excluding the lake extensions or protrusions (narrow penetrations into land) as compared to the original image and field checks. $NDWI_3$ estimated the shoreline in a way that included the protrusions, mostly shallow water, with different pixel values, such that it is up to the user to apply detailed thresholding to define the true water pixels. This leaves the question of precise shoreline still open and the arguments presented for portion A apply to portion B for $NDWI_3$. $NDWI_3$ gave nearly similar results as $NDWI_1$ with evidence of varied degrees of underestimation and overestimation of the shoreline. $NDWI_5$ overestimated the water body, including non-water pixels as water pixels. From this empirical evaluation, $NDWI_3$ gave the best NDWI result for this section of the lake, although it underestimated the shoreline in most cases, but included the complicated portions.

The TCW results in figure 4(*f*) delineate the detailed structure of the shoreline and, as observed in scenario A, the precise boundary is not perfectly defined or visible. Compared to $NDWI_3$, TCW gave better results in estimating the complicated shoreline. However, overall, TCW gave better results in this portion than the NDWIs, as it approximated the narrow lake portions that encroached into land very well.

3.5.3 Lake–mountain interface (portion C). In the third analysis, an edge strip was analysed (portion C). The edge was taken along the steep mountain (land)–water intercept (cliff) on the eastern side of the lake. This portion presents a sharp edge and is a good indictor for shoreline estimation because of the sharp intercept between water and land. However, shadow and other effects may prevent complete distinction between the land and water. Figure 5(*a*) shows the original image. The results for portion C are presented in figures 5(*b*)–5(*e*), respectively, for $NDWI_{2–5}$.

The point of evaluation in scenario C is based on the ability to estimate the shoreline. This seems to be achieved by all the NDWI results except for $NDWI_5$, which overestimated the true shoreline by including non-water pixels, as in the adjacent mountain, as water pixels. $NDWI_2$ and $NDWI_4$ gave very similar results with fuzzy shoreline characteristics. The best shoreline delineation among the NDWIs was achieved by $NDWI_3$.

The TCW results are presented in figure 5(*f*). Comparing TCW results with the NDWIs, TCW defined the mountain–water shoreline more accurately, although not crisply. The shadow effects and other spectral interferences could have introduced this. The TCW results are comparable to the $NDWI_3$ results except that $NDWI_3$ present a sharper shoreline estimation than TCW. $NDWI_3$, however, slightly underestimated some portions that were correctly defined by TCW, indicating that the sharpness of the shoreline does not necessarily imply higher accuracy.

From all the above results, it is consistently observed that $NDWI_3$ and TCW gave the best results. Conclusively, the assessment of portions A, B and C indicate that TCW gave the best results, followed by $NDWI_3$. $NDWI_3$ delineates the optimal boundary with both slight under- and overestimation compared to TCW. TCW includes all the water pixels with minimum errors of omission and commission. This indicates that a combination of the two methods may result in better information for a more robust delineation of the shoreline. This is the rationale of this research. The

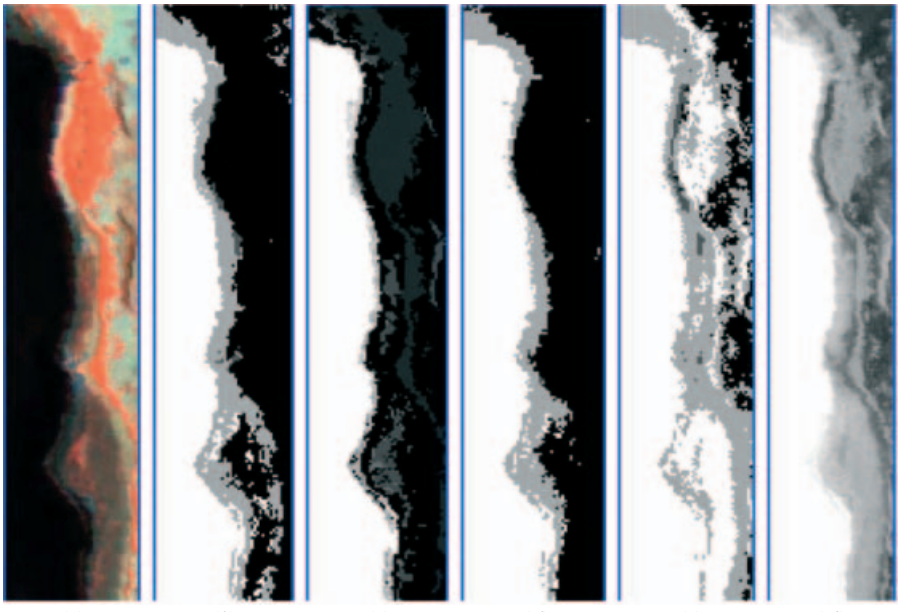

Figure 5. (*a*) Location of test area C in FCC; (*b–e*) results of $NDWI_{2-5}$ and (*f*) TCW of Lake Nakuru.

combination of these indices is termed the Water Index (WI), to avoid confusion with other similar existing indices.

3.5.4 Reliable and unreliable edge information. The above results only considered the edge information for the 'true-edge' for reliable change detection reasons. However, the shallow edge information, that is all the water at a given instantaneous time, can also be mapped by combining the buffer zone with the 'true-edge'.

Note that if the shallow edges are to be included as part of the true lake edges, then from the results in figures 3 and 4, $NDWI_2$ and $NDWI_4$ have to be compared for the most informative or relevant NDWI. This is because by empirical evaluation, these indices present the most informative shallow-edge buffer zone. Then the combination of the suitable NDWI and TCW is made and the threshold for the optimal number of pixels to include is applied. The result of this analysis is demonstrated in §4.6.

4. Water Index (WI)

Following empirical analysis of the results, TCW gave better results than either of the NDWIs. However, the problem of a clearly defined shoreline is persistent in both the results; that is, crispness does not imply higher accuracy and fuzziness does not necessarily mean lower accuracy. Striking a balance between these two observations is a way forward to accurate shoreline detection from remote sensing data. A new WI has been proposed that combines the TCW and $NDWI_3$ to accurately delineate the water body.

The logic to this approach is threefold. (1) The TCW by itself does not normalize the wetness index coefficient. This implies that TCW may contain irrelevant pixels despite being a weighted index, implying that the weights used in the TCW

Table 1. Rule sets for the Water Index (WI) based on TCW and $NDWI_3$.

	TCW	$NDVI_3$	WI (rules)	Notes/remarks
Rule 1	Yes	Yes	Yes	Cross-hairs (figure 7(*a–c*))
Rule 2	Yes	No	Yes	
Rule 3	No	Yes	Yes (if water DN=DNTCW ± 1) No (else)	Point #1 (figure 7(*d–f*))
Rule 4	No	No	No	Every point outside the boundary defined as water by TCW and $NDWI_3$

TCW, Tasseled Cap Wetness; NDWI, Normalized Difference Water Index; DN, digital number.

computation for each band reflectance may not fully explain the land–water interface separation; thus additional complementary information is essential. (2) The NDWI introduces the normalization effect, by taking the ratio of the difference to the sum, which can in turn be used to fix the boundary in some logical way through comparison with and according to TCW. (3) The choice of band 5 and band 4 ($NDWI_3$) among the NDWIs is supported by the fact that band 5 has the highest weight even in the computation of TCW (equation (1)). This indicates that band 5 is the most significant band in land–water interface separation. The proposed WI is presented in equation (7) as a combination of equations (1) and (4). (Note that the WI is computed in unsigned 8-bit mode.) Although these indices are not new, their combinational approach as identified in this study is considered to be more useful than if used independently as in previous studies (e.g. Frazier and Page 2000).

$$\mathrm{WI} = f(\mathrm{TCW} \pm k, \mathrm{NDWI}_3) \tag{7}$$

where k is a constant that can be varied based on the rules and its choice depends on the spatial resolution of the sensor and f denotes a function. A set of rules established for the computation of WI are presented and illustrated in table 1. It is worth clarifying that for the 'true-edge' information mapping, the rules presented in table 1 are biased based on TCW for water identification and NDWI for masking non-water pixels in the WI computation.

The results of WI based on Lake Nakuru are illustrated in figures 6(*a*) and 6(*b*) for the Landsat TM and ETM+, respectively. The results show perfect shoreline definition and water body isolation from the rest of the scenes. Figures 6(*c*) and 6(*d*) for TM and ETM+ showing the mountain–lake shoreline, which was fuzzily represented before by the TCW and NDWI (figure 5), are now perfectly isolated. In §4.1 the rationale for the combination is described. The WI results are then analysed using geometric collocation assessment and scatter plot comparison of the fusion between TCW and $NDWI_3$.

4.1 *Geometric collocation and combination rule*

Taking a portion of each of the three results, $NDWI_3$, TCW and WI, we demonstrate the concept of the geometric collocation accuracy analysis by identifying and following similar points on conjugate images. We extend this section to explain how the combination of TCW and $NDWI_3$ is achieved. Figure 7 shows the example with cross-hair intersection and point #1 common to the three images.

At the cross-hair point (lower-left pixel) (figure 7(*a–c*)), the spectral reflectance is the same, that is water in TCW and $NDWI_3$, hence water in the WI. We call this rule

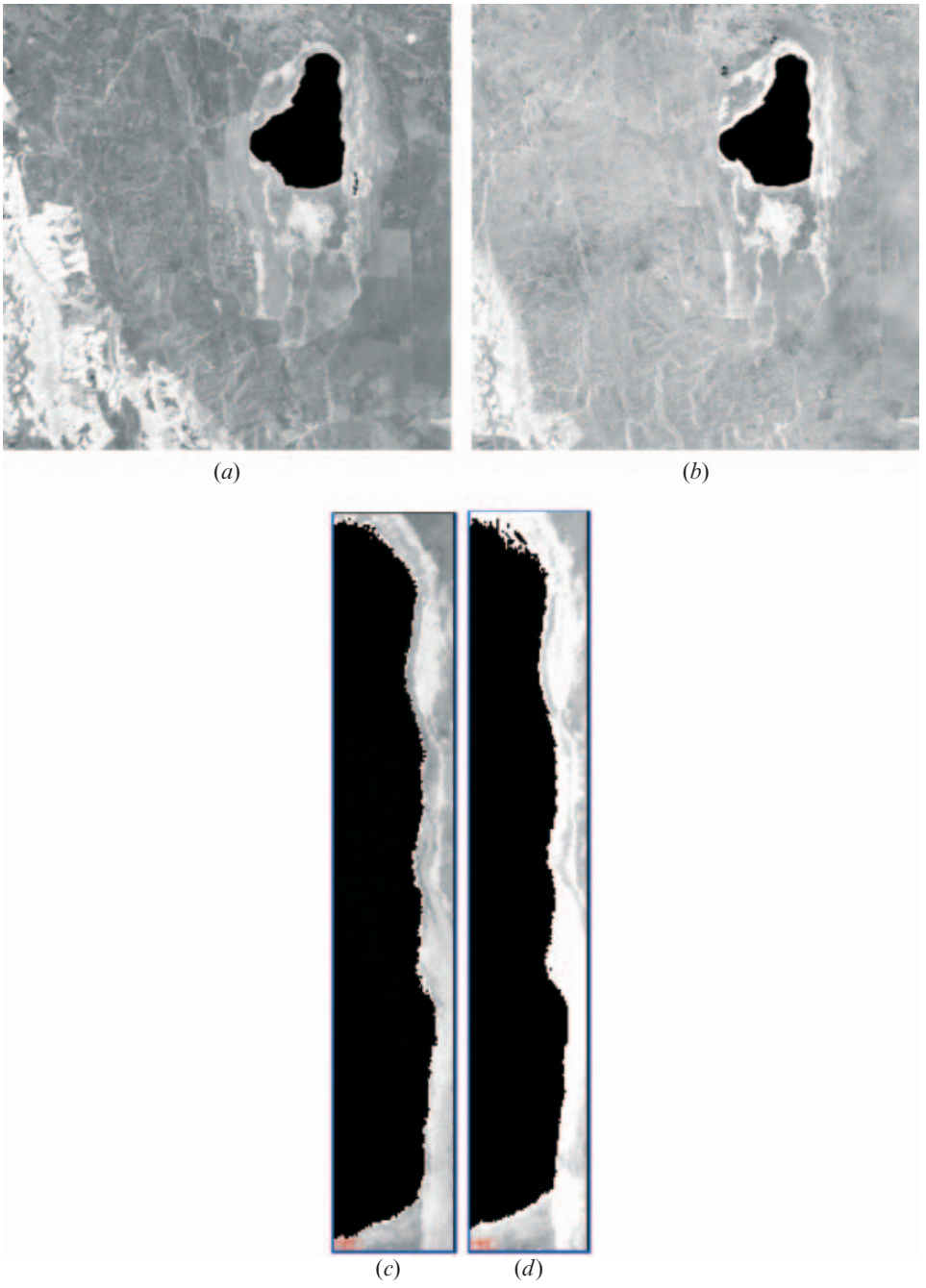

Figure 6. Results of WI from (*a*) TM data and (*b*) ETM data over Lake Nakuru. (*c, d*) Eastern part of Lake Nakuru.

1 or scenario 1. As TCW is a better estimator of the shoreline than $NDWI_3$, we model the new shoreline according to the following conditions or rules based on empirical investigations and field verifications (table 1).

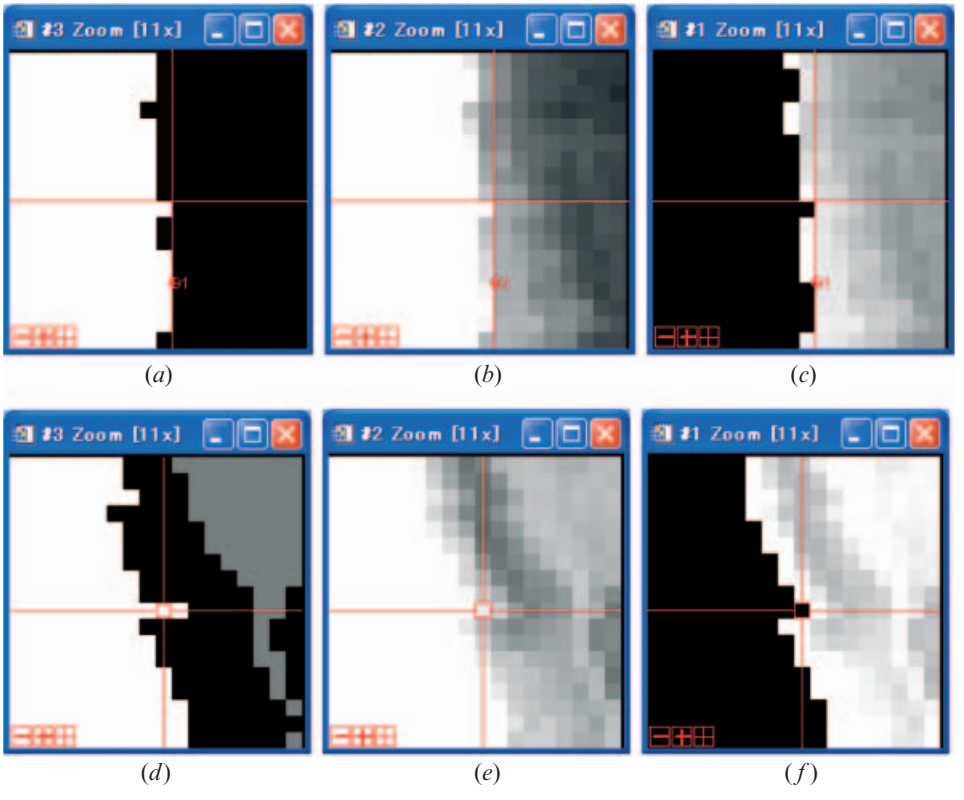

Figure 7. Illustration of WI rule using NDWI and TCW. (*a–c*) Rule 1; (*d–f*) rule 2.

The DN representing water is determined empirically and is denoted as $DN_{TCW} \pm 1$ for TCW and DN_{NDWI} for $NDWI_3$. Because of the fuzziness of the shoreline determined by TCW, we empirically determined the ($k = \pm 1$) value to correctly define the shoreline based on the neighbouring pixels to DN_{TCW}. Note that the (± 1) also represents a single pixel that is equivalent to 30 m × 30 m. This basic threshold is brought in because of the observed lake water characteristics in the narrow protrusions into the land. The set of rules that were automatically implemented are summarized in table 1. The rationale for constructing table 1 is self-explanatory in that water pixels are obtained if they are determined as water pixels both in $NDWI_3$ and in TCW and/or if they fall within a threshold set for TCW water pixels.

By combining the common points based on the above set of rules, perfect shoreline with exact geometric correction is defined with WI as the result. It is evident from figure 7 that the WI results pose a 100% spectral separability from the neighbouring and/or entire scene pixels. The analysis of the results shows that the WI proposed in this study is more promising for lake delineation than the independent methods previously used in other studies. This is a significant finding for any kind of further spatial analysis of water systems, as physical mapping is the first step in any water resource studies. Through on-screen control point comparison in image-to-image mode, the fusion of the two shorelines was found to be perfect in accordance with the rules in table 1. As already cited, the 'mother' indices are not new; however, their combinational approach as identified in this study is considered to be more

useful than if used independently as in previous studies (e.g. Frazier and Page 2000). In other words, the combined results have more weight and accuracy for mapping the lake water body.

4.2 *Assessment of WI results using a 2D scatter plot*

Using a 2D scatter plot, we determined the possibility of extracting water bodies from Lake Nakuru between 1986 and 2001 using the $NDWI_3$, TCW and WI as independent methods. From the scatter plots (figure 8), the following observations were made: (a) using $NDWI_3$, the separability of water bodies from other scene features is very low as depicted by the close clustered points in the feature space. (b) In the case of TCW, the Euclidian distance between the water pixels and other scene pixels are fairly separable, more so compared to $NDWI_3$. However, few non-water pixels are very close to the determined water feature space. (c) WI clearly takes the advantages posed by the 'mother indices TCW and $NDWI_3$' and perfectly separates the water pixels from the rest of the scene features. It exhibits a large Euclidean distance of separability that curves out the water from the rest of the features. This is the phenomenon that formulates the hypothesis of this study. Even though the 2D scatter plot depends on the look-up scale table or stretch used, it may serve as a useful indicator for separability to some degree.

4.3 *Geometric accuracy assessment and comparison*

To validate the accuracy with which the shoreline was delineated using the three methods, $NDWI_3$, TCW and WI, a 3-day DGPS coordinate mapping campaign around Lake Nakuru shoreline was carried out by three groups. Although each group had its extent determined, it was agreed to overlap each other's area of coverage such that redundancy in some of the measured points was used to assess the accuracy of the measurements in general.

More than 200 points were collected and 167 of the points were established as reliable for the geometric accuracy assessment. Of these points, 67% were located on the more gentle western side of the lake. A linear regression plot was then generated between the ground points and the test scene ETM + $NDWI_3$, TCW and WI results. The regression plots were generated by computing and comparing the absolute root mean square errors (ARMSEs) between the point coordinates derived by DGPS observations and those of the study results. Figure 9 shows the regression plots of (*a*) $NDWI_3$, (*b*) TCW and (*c*) WI upon the ground points.

The lowest regression ($R=0.55$) was observed for $NDWI_3$, followed by $R=0.74$ for TCW and $R=0.98$ for WI. Given that the DGPS observations were made during the satellite overpass period close to 3 April 2001, the linear regression of the shoreline observation from the satellite data and the ground observation shows that there was a match between the DGPS measurements edge information and the satellite-derived edge information. The best match of the regression fits was that from the proposed approach of WI, followed by TCW and then $NDWI_3$. These results also counter confirm the 2D scatter plot observations.

4.4 *Change detection using WI results*

The second objective of this research was to estimate the surface area and hence determine the change in the sizes of the five lakes between 1986 and 2001. For change detection, the results of the WI were used (figure 6(*a, b*)). As the precise lake

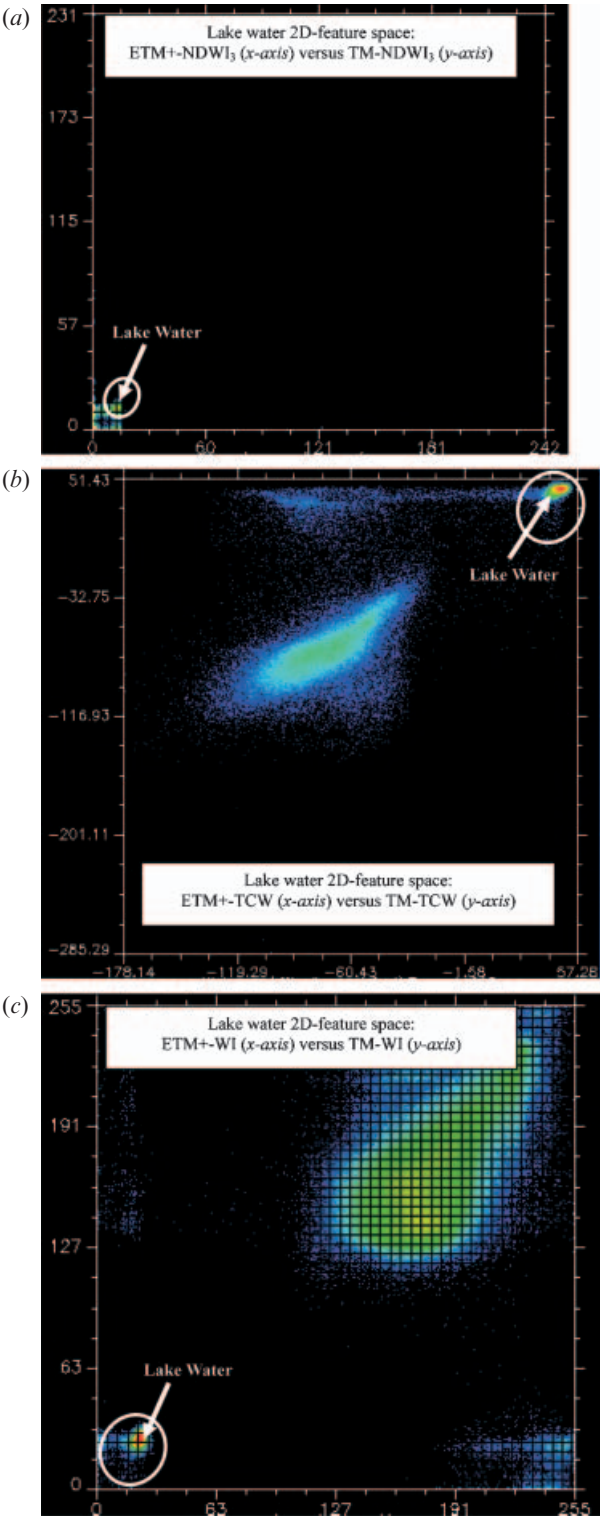

Figure 8. Two-dimensional feature space of the Lake water in NDWI using TM and ETM data for (*a*) NDWI; (*b*) TCW; and (*c*) WI.

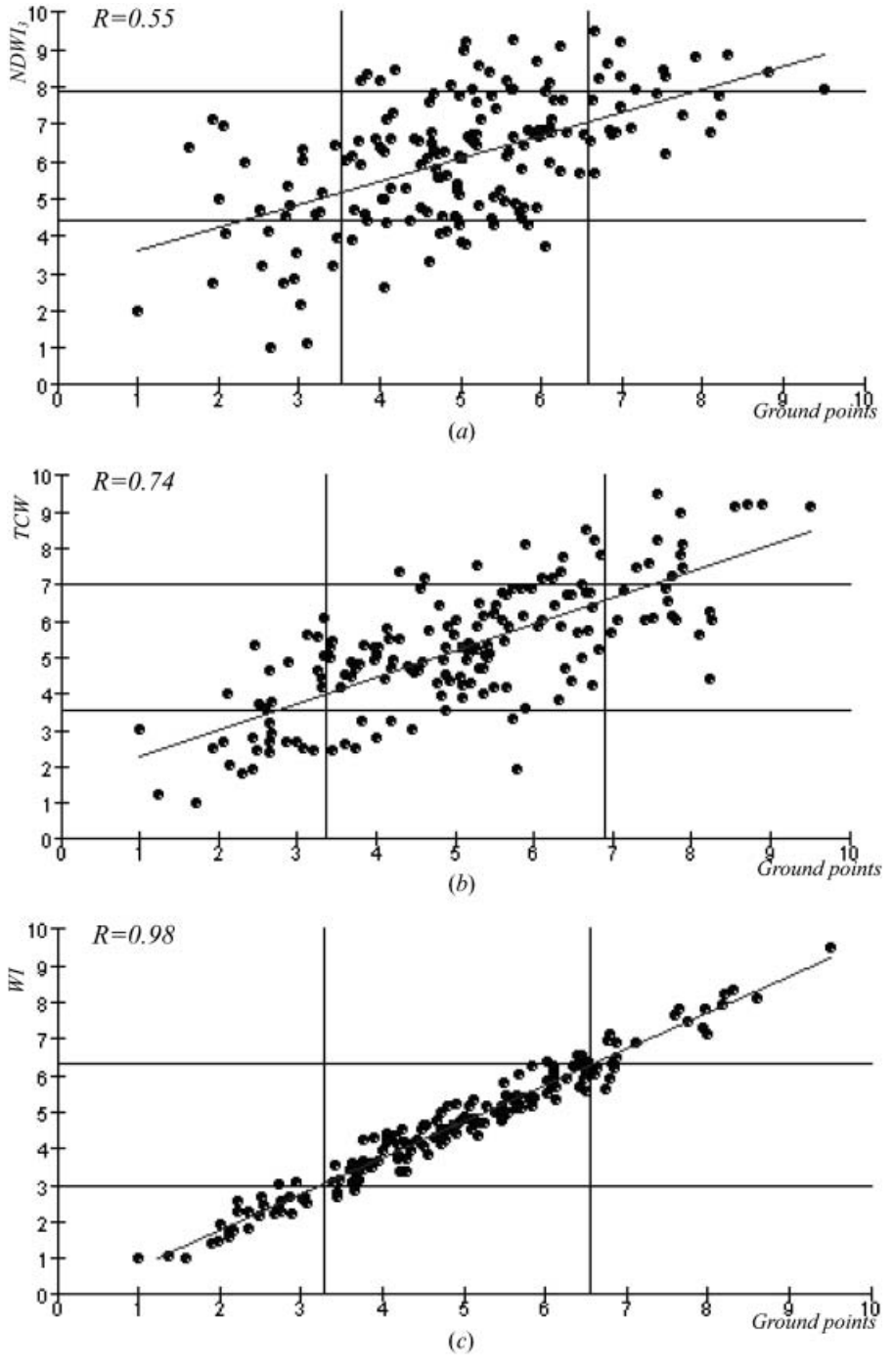

Figure 9. Linear regression of shoreline identified by DGPS with (*a*) NDWI; (*b*) TCW; and (*c*) WI.

boundary has been defined, the exercise of lake surface area change detection is now straightforward. Thus, a direct image differencing was applied (equation (8)) between the two dates:

$$\mathrm{DI} = I_{\mathrm{WI86}} - I_{\mathrm{WI01}} \tag{8}$$

where I_{WI86} and I_{WI01} are the water indices for the 1986 and 2001 images, and DI is their difference.

The assumption in image differencing is that the unchanged pixels will have a zero difference in DN value and as the two images were normalized, the same is expected throughout the scene. The changed areas are highlighted in the DI image. Looking at the results from figure 6(*c*) and 6(*d*), it is clear that the change in shoreline will be distinct from the rest of the scene features. This implies that there is no editing of the change/no-change information, that is, the value representing lake water change will be a single unique DN value. This DN value can be determined by either density slicing or unsupervised classification; both techniques gave the same results for identifying the changed pixels for the water body in the test scene of Lake Nakuru.

The change detection results for the Lake Nakuru test scene are presented in figure 10(*a*). Within the test scene, the results were analysed for surface area change accuracy. Some of the depicted changes are not associated with the lake itself, that is errors of 'omission' and 'commission'. Note that the omission and commission errors are not used here from the classification results analysis point of view, but rather in the inclusion and exclusion sense. Attempts using two counter-methods to validate the true lake size were investigated. First, an automatic threshold based on size was applied such that if the total size of a group of pixels at the examined date was less than that of the estimated lake size, then they were eliminated from the scene. This is straightforward as the lake is far larger than any other enclosed features within this scene. To check the accuracy of this first approach, a constant lake size was determined by iterative standard deviation selection, while performing region growing within the lake in the original Lake Nakuru images (figure 6(*a, b*)). The grown area is subtracted from the entire scene and the true lake size defined. Both methods gave similar results. In figure 10(*b*), the true water pixels are differentiated from the error pixels to estimate the true lake size and subsequently its surface area change. The results were that the true change in Lake Nakuru was estimated at 2.4858 km^2. The same approach was applied to the five lakes simultaneously and a summary of the results is presented in figure 11 and table 2, and in §4.5.

Figure 11 shows the results for ETM-NDWI (*b*), ETM-TCW (*c*), ETM-WI (*e*) and TM-WI (*d*) with ETM False Colour Composite (FCC) over the study area. Table 2 gives a summary of the corrected lake area data for the five lakes.

4.5 *Brief assessment of lake-type change vector*

Analysing the observed changes in terms of lake-type change vector (decrease/increase), expressed as area percentages from figures 12 and 13, the following observations were made:

(a) The saline lakes, Bogoria, Nakuru and Elementaita, although the smallest in size of the five lakes compared, showed the least change vector (decrease in size) of 4.80%, 6.58% and 11.61%, respectively. Lake Elementaita, however, with an area of less than half the size of these saline lakes, had the highest change vector. Lake Nakuru had a higher surface area change than Lake Bogoria, although both are of nearly the same size.

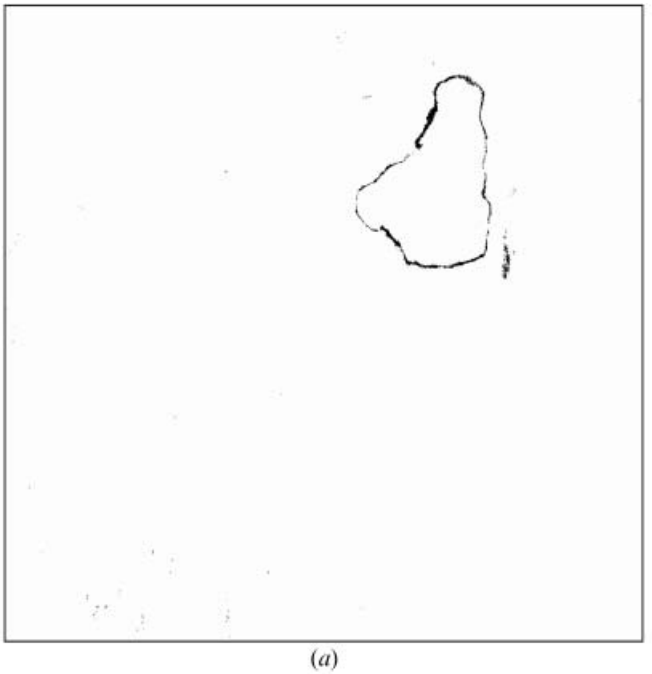

(*a*)

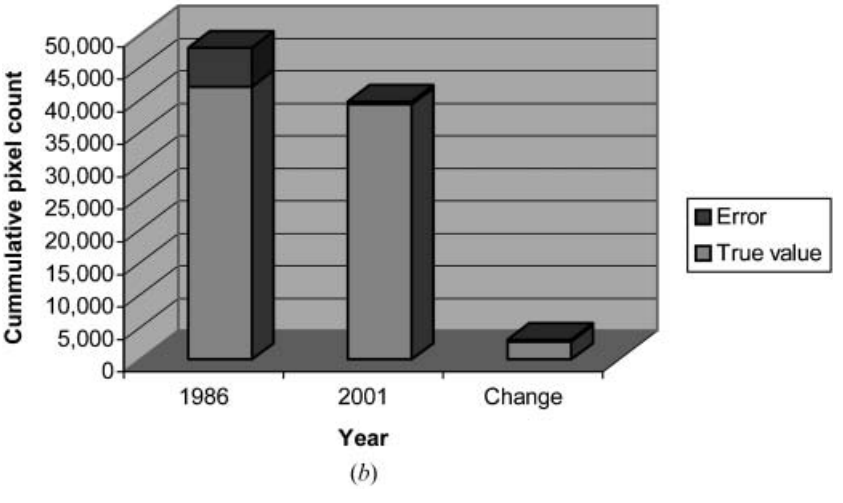

(*b*)

Figure 10. Change detection of (*a*) WI and (*b*) the results of accuracy from 1986–2001 over Lake Nakuru.

(b) The non-saline lakes, Baringo and Naivasha, the two largest of the five lakes, exhibited the largest change vectors of 14.23% and 17.96%, respectively. Lake Baringo, although slightly smaller than Lake Naivasha, depicted a changed area that was less than that of Lake Baringo.

(c) Following from (a) and (b), from Lake Bogoria going south, the decrease in the sizes of the lakes increases, as depicted by the change vectors.

(d) The lakes ranked in size, with respect to the 1986 statistics as the base, from largest to smallest were Baringo, Naivasha, Nakuru, Bogoria and Elementaita. However, comparing the individual lake size change ratios,

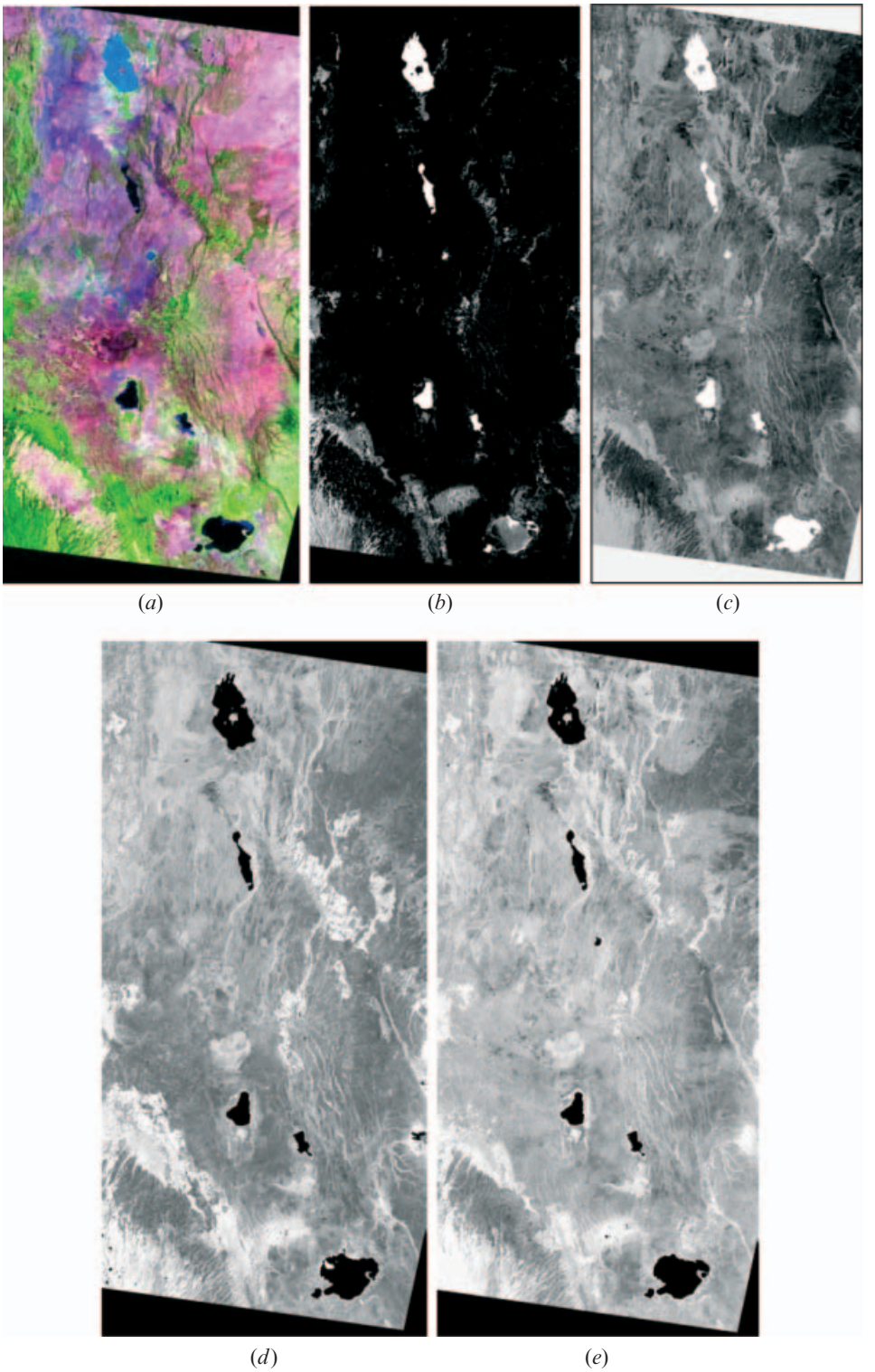

(*a*) (*b*) (*c*)

(*d*) (*e*)

Figure 11. Results of (*b*) ETM-NDWI; (*c*) ETM-TCW; (*d*) TM-WI; and (*e*) ETM-WI with ETM FCC over the study area.

Table 2. Corrected lake area data.

	Baringo		Bogoria		Nakuru		Elementaita		Naivasha	
Year	PC	Area (km^2)	PC	Area (km^2)	PC	Area (km^2)	PC	Area (km^2)	PC	Area (km^2)
1986	153 979	139	37 029	33.3261	42 000	37.8000	18 130	16.3170	152 545	137.2905
2001	132 074	119	35 253	31.7277	39 238	35.3142	16 026	14.4234	125 144	112.6296
DI	21 905	20	1776	1.5984	2762	2.4858	2104	1.8936	27 401	24.6609

PC, pixel count; DI$=I_{WI86}-I_{WI01}$, as defined in equation (8).

we observed the following order: Naivasha, Baringo, Elementaita, Nakuru and Bogoria in an increasing fashion. We note here that the saline lakes changed more with respect to their original surface areas than the non-saline lakes.

4.6 *Shallow lake edge mapping*

The above results focused on change detection based on non-dynamic edge information. To map the shallower dynamic edges of the lake, equation (7) was modified to equation (8) as follows:

$$\mathrm{WI_{se}} = f(\mathrm{TCW} + x,\ \mathrm{NDWI_2} + y) \tag{8}$$

where se means shallow-edge, and x and y refer to the DN values of the buffer zone in TCW and the chosen NDWI, respectively. The values for x and y are flexible in choice and range and depend upon a particular scene. In this case $NDWI_2$ was preferred to $NDWI_4$, even though they do not present significantly different results, probably because the band 2 that is common to these indices plays a significant role in detecting the mixed water/suspended solids shallow edge. This is in part a motivation for the rationale of testing the indices.

The results demonstrating the shallow water mapping for Lake Nakuru using ETM+ are presented in figure 14 for the western flat section of the lake with the shallow edge. The same set of rules as in table 1 are applied except that in this case

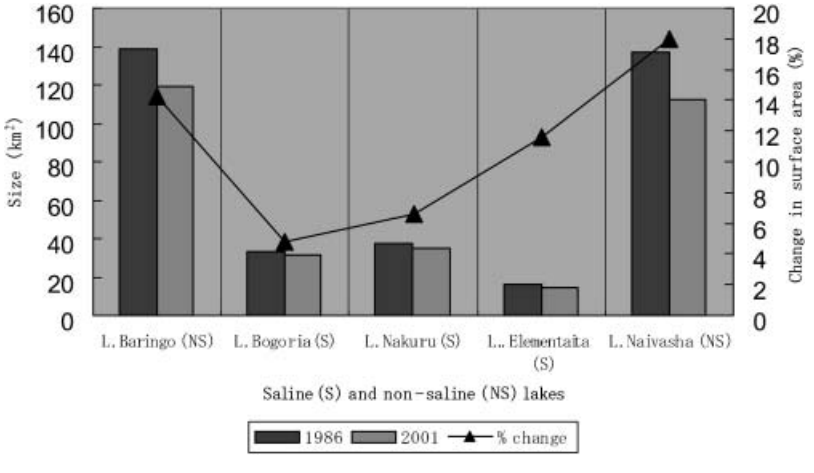

Figure 12. WI-based surface area of lakes studied for 1986–2001.

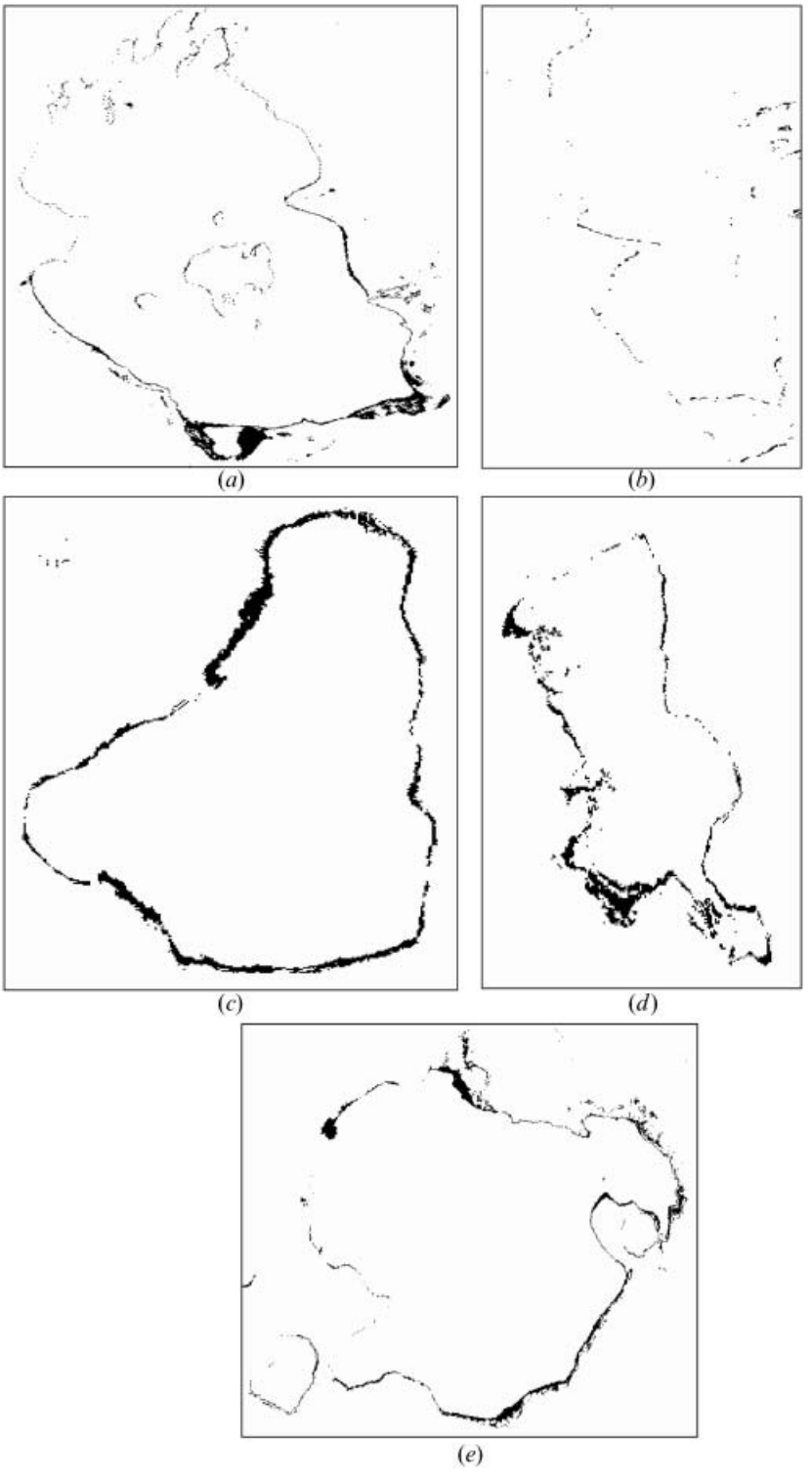

Figure 13. Change in water spread in 1986 and 2001 for (*a*) Lake Baringo; (*b*) Lake Borogia; (*c*) Lake Nakuru; (*d*) Lake Elementaita; (*e*) Lake Naivasha.

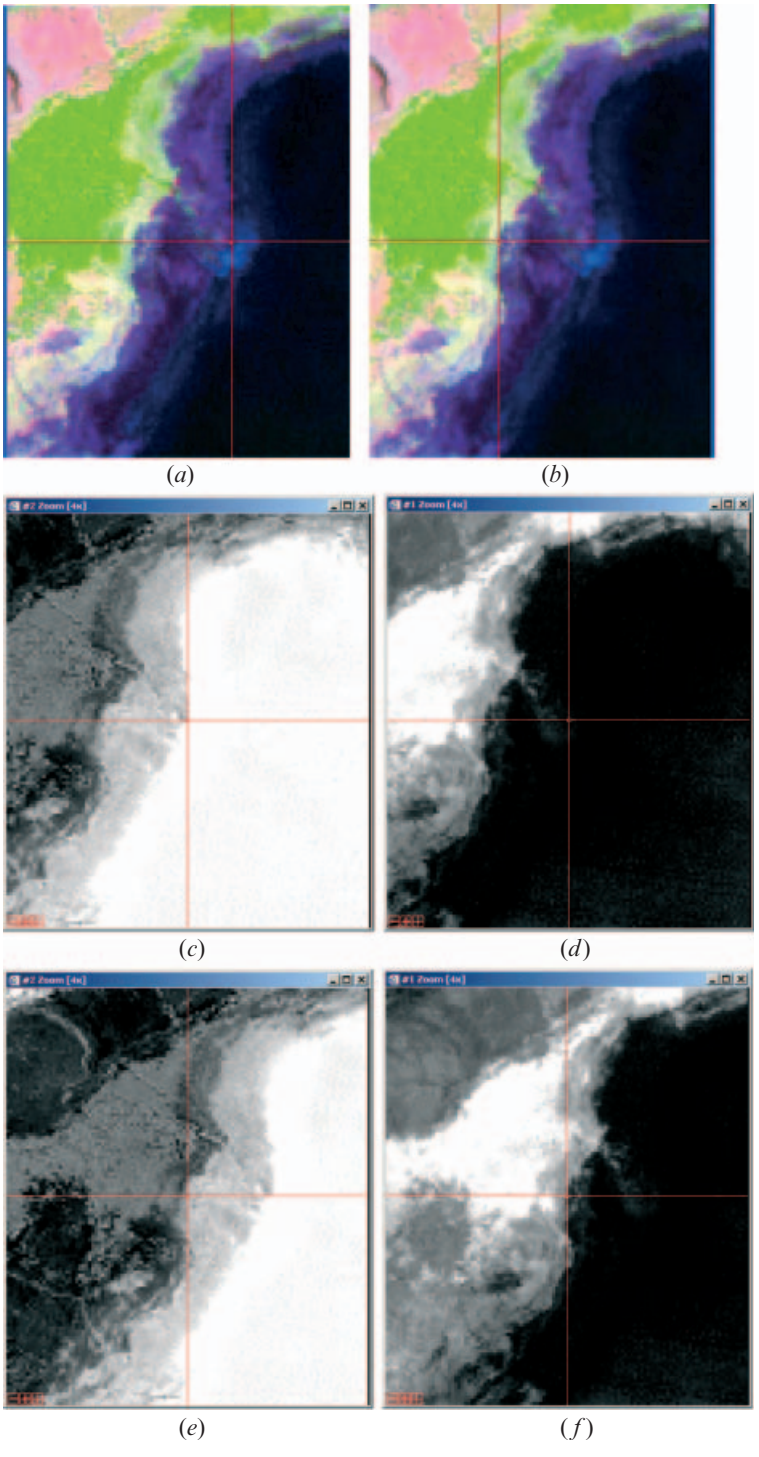

Figure 14. Illustration of shallow edge information extraction showing the edge position for TCW results for (*a*) before and (*b*) after WI_{se} adjustments (*c, e*) Edge information from TCW: (*c*) before and (*e*) after WI_{se} adustments. (*d, f*) depiction of edge position after WI_{se} was applied.

the optimal NDWI is different and the thresholds were determined as $x=-6$ to -40 and $y=2$. These thresholds depend strongly on the physical and chemical characteristics of the scene at the time of measurement. Figure 14(*a*) and 14(*b*) depicts the edge information as determined from TCW and the WI_{se}, respectively (cross-hair points). Note that the buffer for $NDWI_2$ is constant ($y=2$) round the lake and hence can be straightforward to interpret. From figure 14(*a*) or 14(*b*), it is evident that there is a very shallow edge (mixed bluish/dark (indigo) pixels – unreliable edge), a shallow edge (bluish pixels – considered as the 'true-edge' for change detection) and a deeper edge (dark pixels – pure water body) on moving from the left to right across the water body. The common cross-lines in figure 14(*c*) and 14(*d*) shows the position of the edge in the TCW image and in the WI_{se}-derived image. In figure 14(*e*) and 14(*f*), the adjusted edge to include the shallow portions is presented. In this case of shallow edge mapping, the selection of x and y values depends on which location the analyst considers as the appropriate edge. The WI_{se} results are only used for illustration of how and where shallow edges can be mapped.

5. Discussion

5.1 *Lake water body mapping and change detection*

Referring to the literature review in the introduction, previous studies reported that thresholding of band 5 and band 7 and together gave good results. In this study, normalization of these bands ($NDWI_1$) gave the worst results. This clearly indicates that a combination of the two bands by normalization does not yield good results for our case study. This implies that a combination of the SWIR bands is not suitable if assessed or combined by normalization. However, if the weights of their contributions are combined in TCW, their significance is realized (by introducing the weights of 0.7112 and 0.4572, respectively, for bands 5 and 7). This indicates that a direct combination of the two bands might give better results than their normalization.

In order of performance magnitude, $NDWI_1$ was ranked last, followed by $NDWI_5$, $NDWI_4$, $NDWI_2$ and finally $NDWI_3$ in increasing order of performance. This order of performance may be explained as follows. The ranking of $NDWI_3$ in first position implies that the MIR and NIR bands 5 and 4, respectively, are the most significant for land–water identification with respect to normalization from the entire visible, IR to SWIR optical portions of the electromagnetic spectrum. This also implies that the Landsat visible and SWIR bands are not as significant as the NIR and MIR bands. A similar argument explains the performance of $NDWI_2$, $NDWI_4$ and $NDWI_5$. Conclusively we observed that the MIR and NIR bands are most suitable for this task, followed by NIR and the green band, then MIR and the green band, the SWIR and the green band, and finally MIR and SWIR band combinations.

To further explain the observation above, in the visible electromagnetic spectrum, water, vegetation, shadow and land all have relatively high spectral reflectance. This means separating water from the other predominant features within the visible region may not be very feasible, and this was not tested in our study. In the NIR and SWIR, water exhibits the lowest spectral reflectance compared to land and vegetation. In the SWIR (bands 5 and 7), the spectral reflectance from water is nearly zero, while land is at its peak of reflectance and vegetation also has a

relatively high reflectance. The NIR and SWIR portions are thus the best to use in separating water from vegetation and land as reported for the 'true-edge' detection.

From the water bodies detection and exact shoreline delineation, change detection followed. All NDWIs gave very closely related results. Therefore, a redundant reliable observation was necessary to counter-check the results; motivating the comparison of the NDWIs to find out which one captures most accurately the edge information. The results showed that inclusion of the visible region (band 2) was suitable for mapping the shallow water regions more accurately, while for the 'true' lake edge, as in our interpretation, the infrared bands (5 and 4) were instrumental. Band 7, although located in the MIR, was found not to be significant in either shallow water body mapping or deep water edge delineation as observed in the $NDWI_5$ results.

The high regression by WI can be explained by the relatively higher spectral separability compared with both TCW and $NDWI_3$. WI showed that the shorelines were detected with an accuracy of 98.4%. This is 22.33% higher than the TCW results, and 43.19% more accurate than the $NDWI_3$ results. The combinational approach (WI) presented in this study is suitable in the sense that it not only enhances the desired lake water body but also maps the shoreline more accurately than the independent TCW and NDWI methods. The results of WI made the change detection process a simple, fast and straightforward exercise for a wide area, that is one scene of Landsat, with different lakes (saline and non-saline). This advantage was brought about by the selection of suitable bands and the inclusion of weighted transformation and normalization techniques together, leading to automatic shoreline thresholding.

The results of the change vector analysis indicate that under natural conditions (without human influences) the changes in the lake area may be dependent on the salinity and non-salinity and may not necessarily depend on the size and location. We note that the saline lakes changed more with respect to their original surface areas than the non-saline lakes even though they were the smallest in size. This observation requires a much more detailed ecological study and is not within the scope of this study. Each lake has to be analysed in detail first before generalization or making specific conclusions.

With the absence of MIR/SWIR bands in the new high-spatial resolution sensors, such as QuickBird and IKONOS, the method proposed in this study may not work directly. Thus alternative methods to address the uniqueness of these new datasets (i.e. low-spatial resolution and high-spatial resolution) are being sought. Landsat presents a good tool for water body mapping because of lower costs, higher instantaneous field of view (IFOV), better spectral resolution and the fact that the fluctuation of some shorelines are normally very high, such that its monitoring them at, say, 1 m may not be suitable.

5.2 *On the Rift Valley lakes and their dynamism*

Many environmental risks to East African Rift Valley lakes arise within their catchments and can be addressed by riparian states or lakes in the catchments through appropriate basin management initiatives. However, other risks that arise from atmospheric change can affect lakes over broad areas and will require regional or even global action. There is now evidence that climate change, intensifying land use (mobilizing nutrients) and toxic substances are increasingly affecting the atmosphere over the lakes. The lakes are particularly sensitive to these changes

because of their enormous surface areas, slow flushing rates and the importance of direct rainfall in their water budgets. Their response times may be slow to yield a detectable change, and unfortunately recovery times may also be slow.

It is possible for atmospheric effects to act antagonistically to impacts of catchment change (e.g. evidence for lower productivity in different lakes despite ongoing catchment degradation) but antagonistic effects may become synergistic in the future (e.g. the positive effect that increasing atmospheric sulfur deposition might have on mercury methylation). Improved understanding of the physical dynamics of these lakes, and models to link their physical and biogeochemical behaviour to regional, meso-scale climate models, will be necessary to guide lake managers.

Each lake differs from the other with respect to limnology, catchment dynamics and human impact. However, one thing in common to all the lakes is that they face unprecedented differentiating pressures from a variety of human-related activities. The crucial issues facing the lakes include rapid riparian population growth, unsustainable exploitation of fisheries and other living resources (overexploitation), pollution—microbiological and chemical, eutrophication, suspended soils arising from deforested catchment areas, fresh-water shortage, global change, habitat and community modification. The rapidly evolving ecological changes occurring in these lakes threaten their survival as sites of great human heritage and may alter permanently their ecosystem function and overall biodiversity.

Human activities are affecting the lakes directly or indirectly. Global climate change resulting from greenhouse gases may have started to affect the lakes. It is concluded that deterioration of the Rift Valley lakes has in general resulted from the following major causes:

(1) Rapid population growth of the riparian communities with concomitant rapid expansion of urban centres.
(2) Large demand of export markets for fisheries with no improvement in fish handling capacities and technologies.
(3) Lack of compliance to and enforcement of legislations governing the fishery industry and environmental pollution.
(4) Weak regional integration of legal and institutional implementing mechanisms or sustainable ecosystem management.
(5) Low level of community participation in ecosystem management due to lack of education and public awareness of issues.

6. Conclusions

Automated shoreline data extraction from remote sensing multitemporal imagery is difficult because of the effects of trees and shadows, shoreline structures, low water–land contrast and other factors. The current study presents an approach for 'true lake edge' information extraction and change detection from Landsat TM/ETM+ data series. The results of this work demonstrate that in the case of fast mapping of changes in open water, such as lakes, a combination of TCW and NDWI3, called the water index (WI), can be applied to multi-date data such as 30 m spatial resolution Landsat 7 ETM+ and Landsat 5 TM. Evaluation of the results through rigorous empirical and statistical comparisons demonstrates that the shoreline extracted is promising when applied in the simultaneous analysis of the differences

in the surface areas of the five lakes within the Rift Valley between 1986 and 2001. WI, upon regression analysis with the ground-estimated shoreline of Lake Nakuru, detected the shorelines with an accuracy of 98.4%, which was 22.33% higher than the TCW results, and 43.19% more accurate than the $NDWI_3$ results. The results of the change vector analysis indicate that the changes in lake area may be dependent on the salinity and non-salinity and do not necessarily depend on the size and location. We note that the saline lakes changed more with respect to their original surface areas than the non-saline lakes. This requires more research and is not within the scope of the current study. Further studies, including socio-economic and biogeochemical analysis introducing 3D mapping of the lakes, with shorter intervals of monitoring for spatial–temporal sensitivity and impact assessment, are being considered.

Acknowledgements

This project was funded through the Japanese Ministry of Science and Education fellowship. We thank T. G. Ngigi for accurate work in the geometric and radiometric corrections.

References

Bagli, S. and Soille, P., 2003, Morphological automatic extraction of coastline from pan-European Landsat TM images. In *Proceedings of the Fifth International Symposium on GIS and Computer Cartography for Coastal Zone Management*, Genova, October 2003. (GISIG and ICCOPS), pp. 58–59.

Braud, D.H. and Feng, W., 1998, Semi-automated construction of the Louisiana coastline digital land/water boundary using Landsat Thematic Mapper satellite imagery. Louisiana Applied Oil Spill Research and Development Program, OSRAPD Technical Report Series 97-002. Department of Geography and Anthropology, Louisiana State University.

Cohen, W.B., Maiersperger, T.K., Spies, T.A. and Oetter, D.R., 2001, Modelling forest cover attributes as continuous variables in a regional context with Thematic Mapper data. *International Journal of Remote Sensing*, **22**, pp. 2279–2310.

Collins, J.B. and Woodcock, C.E., 2001, An assessment of several linear change detection techniques for mapping forest mortality using multitemporal Landsat TM data. *Remote Sensing of Environment*, **56**, pp. 66–77.

Crist, E.P., 1985, A Thematic Mapper tasseled cap equivalent for reflectance factor data. *Remote Sensing of Environment*, **17**, pp. 301–306.

Crist, E.P. and Cicone, R.C., 1984, A physically-based transformation of Thematic Mapper Data—The TM Tasseled Cap, *IEEE Transactions on Geoscience and Remote Sensing*, **22**, pp. 256–263.

Crist, E.P. and Kauth, R.J., 1986, The tasseled cap de-mystified. *Photogrammetric Engineering and Remote Sensing*, **52**, pp. 81–86.

Di, K., Wang, J., Ma, R. and Li, R., 2003, Automatic shoreline extraction from high resolution IKONOS satellite imagery. In *ASPRS 2003 Annual Conference Proceedings*, May 2003, Anchorage, Alaska.

Fraser, R.N., 1998, Multispectral remote sensing of turbidity among Nebraska Sand Hills lakes. *International Journal of Remote Sensing*, **19**, pp. 3011–3016.

Frazier, P.S. and Page, K.J., 2000, Water body detection and delineation with Landsat TM data. *Photogrammetric Engineering and Remote Sensing*, **66**, pp. 1467–1467.

Jupp, D.L.B., Mayo, K.K., Kuchler, D.A., Heggen, S.J. and Kendall, S.W., 1985, *Landsat Based Interpretation of the Cairns Section of the Great Barrier Reef Marine Park.* The C.S.I.R.O. Natural Resources Series no. 4.

KAUTH, R.J. and THOMAS, G.S., 1976, The tasseled cap—a graphic description of the spectral–temporal development of agricultural crops as seen by Landsat. In *Proceedings of the Symposium on Machine Processing of Remotely Sensed Data*, 1976, Purdue University of West Lafayette, Indiana, pp. 4B-41–4B-51.

MCFEETERS, S.K., 1996, The use of normalized difference water index (NDWI) in the delineation of open water features. *International Journal of Remote Sensing*, **7**, pp. 1425–1432.

MOLLER-JENSEN, L., 1990, Knowledge-based classification of an urban area using texture and context information in Landsat TM imagery. *Photogrammetric Engineering and Remote Sensing*, **56**, pp. 475–479.

NIEDERMEIER, A., ROMANEESSEN, E. and LEHNER, S., 2000, Detection of coastlines in SAR images using wavelet methods. Available online at: www.dfd.dlr.de/projects/TIDE/sar_coastline_paper/paper.html (accessed 23 January 2005).

SCHWÄBISCH, M., LEHNER, S. and WINKEL, N., 2001, Coastline extraction using ERS SAR interferometry. Available online at: http://earth.esa.int/workshops/ers97/papers/schwaebisc/361c.htm (accessed 23 January 2005).

SMITH, L.C., 1997, Satellite remote sensing of river inundation area, stage, and discharge: a review. *Hydrological Processes*, **11**, pp. 1409–1413.

ZHU, X., 2001, Remote sensing monitoring of coastline change in Pearl River estuary. Paper presented at the 22nd Asian Conference on Remote Sensing, 5–9 November 2001, Singapore. Available on CD-ROM, paper no. 322.